Bubble-driven mixer integrated with a microfluidic bead-based ELISA for rapid bladder cancer biomarker detection

Yen-Heng Lin · Chia-Chu Wang · Kin Fong Lei

Abstract In this study, fine bubbles were successfully generated and used as a simple, low-cost driving force for mixing fluids in an integrated microfluidic bead-based enzyme-linked immunosorbent assay (ELISA) to rapidly and quantitatively detect apolipoprotein A1 (APOA1), a biomarker highly correlated with bladder cancer. A wooden gas diffuser was embedded underneath a microfluidic chip to refine injected air and generate bubbles of less than 0.3 mm. The rising bubbles caused disturbances and convection in the fluid, increasing the probability of analyte interaction. This setup not only simplifies the micromixer design but also achieves rapid mixing with a small airflow as a force. We used this bubble-driven micromixer in a bead-based ELISA that targeted APOA1. The results indicate that this micromixer reduced the time for each incubation from 60 min in the conventional assay to 8 min with the chip, resulting in a reduction of total ELISA reaction time from 3–4 h to 30–40 min. Furthermore, the concentration detection limit was 9.16 ng/mL, which was lower than the detection cut-off value (11.16 ng/mL) for bladder cancer diagnosis reported in the literature. Therefore, this chip can be used to achieve rapid low-cost bladder cancer detection and may be used in point-of-care cancer monitoring.

1 Introduction

Cancer is a major cause of death. According to the 2008 World Health Organization (WHO) statistics, there are 7.6 million deaths from cancer every year, accounting for 13 % of all deaths in the population. Of the many types of cancers, bladder cancer is among the top ten cancers in men, is a common urinary tract cancer and has a high recurrence rate (Tanahashi et al. 1978; Li et al. 2011; Lin et al. 2013). The early detection of cancer in the body enables early treatment, which effectively increases the cure rate. Cytology is the main method for cancer detection in hospitals. However, it shows low sensitivity for low-grade bladder cancers (Lotana and Roehrborna 2003; Li et al. 2011). Cystoscopy is frequently used to examine and monitor patients for the recurrence or progression of this disease. However, this detection method is invasive and expensive, and thus leads to increased patient rejection of this option (Mitropoulos et al. 2005; Karakiewicz et al. 2006). Therefore, there are currently many studies that aim to develop highly accurate and rapid but non-invasive ways to detect bladder cancer. Biomarker detection is a very efficient method for this purpose. Recently, researchers found that apolipoprotein A1 (APOA1) in the urine of bladder cancer patients is a biomarker that is highly correlated with bladder cancer. APOA1 is expected to be utilized as a biomarker for the detection of early stage bladder cancer (Chen et al. 2010; Li et al. 2011; Chen et al. 2012; Lindén et al. 2012).

Y.-H. Lin (✉)
Department of Electronic Engineering, Chang Gung University,
Taoyuan 333, Taiwan
e-mail: yenheng@mail.cgu.edu.tw

Y.-H. Lin · K. F. Lei
Healthy Aging Research Center, Chang Gung University,
Taoyuan 333, Taiwan

Y.-H. Lin · C.-C. Wang · K. F. Lei
Graduate Institute of Medical Mechatronics, Chang Gung University,
Taoyuan 333, Taiwan

K. F. Lei
Department of Mechanical Engineering, Chang Gung University,
Taoyuan 333, Taiwan

Microfluidic chips are built on microelectromechanical systems (MEMS) technology that integrates technologies of different fields such as biological detection, electronics, mechanics, optics and sensors (Auroux et al. 2002; Yang et al. 2009b). The small volume of the flow channel allows the reaction to be completed with only small amounts of analytes. In addition, microfluidic chips are portable, suitable for parallel tests and can be easily integrated with automatic control systems due to the small volume of analyte or reagent (Herrmann et al. 2007). Because of the low Reynolds number (Re) of the fluid, the fluid is characterized by laminar flow (Xiao et al. 2006), which prevents effective fluid mixing and causes time-consuming sample mixing. Therefore, there are many studies focusing on the development of a micromixer. In passive micromixers, the channel structures are often altered to improve the mixing efficiency. Kim et al. (2005) designed and fabricated multiple 3-dimensional F-shaped microchannels using the UV-LIGA process. These channels employed two mixing mechanisms, splitting/recombination and chaotic advection, to improve the mixing efficiency of two otherwise difficult-to-mix fluids (Kim et al. 2005). Vijayendran et al. (2003) stacked and connected many L-shaped channel segments, and each segment was rotated 90° relative to its adjoining neighbors. The bends and turns of the microchannel mixed the fluid that passed through (Vijayendran et al. 2003). In addition, micro-blocks were arranged at the bottom of the microchannel, protruding or recessing (Kim et al. 2004). These grooves with fixed intervals were used as barriers to the fluid. Clock-wise or counter clock-wise whirls occurred in the slanted grooves when fluid flowed through and thus achieved fluid mixing. In addition, other research groups have used surface micromachining to fabricate a mechanical stirrer in the microchannel (Lu et al. 2002). The rotor of the stirrer was rotated by the fluid that flowed through it. The above-mentioned passive mixing caused turbulence in the solution to improve the mixing efficiency among the solutions. However, it required complex fabrication processing, which lowers the usefulness of this approach in practical applications. Moreover, the scale of mixing time for the above-mentioned mixer (especial for the staggered herringbone mixer) to achieve approximate 100 % mixing efficiency may take about several seconds and 20 to 40 mm channel length. The mixing speed scale is the same with the proposed bubble-driven mixer. However, in practice, for an ELISA application, the incubation time for biosamples interaction involves much more than two kinds of fluid complete mixing. If the staggered herringbone mixer was adopted for ELISA, a long microchannel might be needed to provide such long incubation time. It may take a large area for the microfluidic chip.

The so-called active mixers require external power to achieve mixing. Suzuki et al. (2004) used a magnetic field to manipulate magnetic beads in the microchannel to disturb the fluid. The embedded electrodes were fabricated and arranged underneath the microchannel to produce an induced magnetic field. However, electrode fabrication requires expensive equipment and complex and time-consuming processing. In another approach, Tsai and Lin (2002) used a resistive heater to heat the fluid in the microchannel and change the fluid's phase from liquid to gas to produce bubbles. The driving force produced by the expanding and collapsing of the bubbles was used to achieve the effect of mixing. However, biochemical analytes such as protein are very sensitive to temperature and will lose activity at excessively high temperature, which limits its practical application. In addition, another fluidic mixing technique, mixing with bubbles, was proposed as a practical technology for use with portable microfluidic devices. Bubbles of gas were introduced into a microchannel and facilitated a laminar stream mixing together through the periodic oscillation of bubbles into left and right channel crosses the streamlines (Garstecki et al. 2006). Another study using similar mixing principle was demonstrated by Mao et al. (2010). Bubbles were generated in laminar stream and passed through an expansion and conversion channel; thus, the bubbles deformed and changed their moving direction, leading to the "stretch and fold" of the fluid. Although this method can rapidly mix two streams, the ability to enhance the incubation of biosamples is not verified. Ahmed et al. (2009) acoustically drove the liquid/air interfaces of bubbles trapped in grooves in the walls of both sides of the microchannel. An acoustic wave of tens of kHz caused high-speed oscillations of the liquid/air interface and thus mixed the fluids rapidly. However, the bubbles trapped on the sidewalls of the microchannels might retain analyte residues, which would result in difficulties in quantifying the samples. Similarly, the so-called cavitation microstreaming generated by applying a sound field on the bubble's liquid/air interface was used to enhance the DNA microarray hybridization. A strong liquid circulation flow arising around a single bubble can be used to effectively enhance fluid mixing (Liu et al. 2002, 2003). Furthermore, McKenzie et al. (2009) fabricated a side microchannel with polydimethylsiloxane (PDMS) to inject gas into the mixing zone. Bubbles were generated in the mixing zone to disturb the liquid. In this design, relatively large bubbles were generated within a micrometer-scale channel. Overflow can easily occur with this method, which thus requires a hydrophobic membrane above the mixing zone. Therefore, there could be a small amount of analyte residue on the membrane, resulting in a reduction in quantitative accuracy.

In this study, a micromixer that is easy to fabricate and straightforward in concept was proposed. This mixer uses extremely small bubbles to disturb the fluid and increase mixing efficiency of the fluid. A wooden diffuser with very fine pores inside can refine the air that passes through it into

groups of bubbles of less than 0.3 mm in diameter. This mixer only requires the driving force of a very small airflow, simplifying the design of the on-chip micromixer. In addition, the microfluidic chip designed for this micromixer was also integrated with a bead-based enzyme immunoassay to quantitatively detect a biomarker that is highly correlated with bladder cancer. The developed microfluidic chip with the bubble-driven mixer is expected to be useful for rapid bladder cancer screening.

2 Materials and methods

2.1 Bubble-driven micromixer principle and chip design

Figure 1(a) is the schematic of the principle of the bubble-driven mixer. Air is injected into the air chamber quantitatively with a syringe pump. A piece of wood (10× 10×3 mm) with a very fine texture is used as a gas diffuser. The air that passes through the wooden diffuser is dispersed into fine bubbles due to the fine pores inside the diffuser, which produce groups of bubbles of less than 0.3 mm in diameter. These micro-bubbles rise from the bottom to the top surface of the liquid due to buoyancy. The rising bubbles cause a disturbance and convection in the fluid in the well and achieve the goal of improving the mixing efficiency. Figure 1(b) is the scanning electron microscope (SEM) image of the wooden diffuser used (Air stone, Berlin Airlift 60, Red Sea, Israel), which is a key component of aquarium equipment. The micrograph reveals that there are many pores of tens of micrometers on the diffuser surface. In addition, we machined the diffuser to a thickness of 3 mm. Therefore, one can imagine that after passing through a 3-mm-long tightly stacked wooden path, the gas would be dispersed into many fine bubbles. In our study, this bubble-driven mixer was also integrated into a microfluidic chip for the rapid detection of a bladder cancer biomarker. The chip design is shown in Fig. 2(a). The chip has four PDMS layers and a wooden diffuser. The top layer contains the mixing and reaction well (2 mm in diameter and 6 mm in depth). A wash buffer channel is connected to the well to extract waste and inject wash buffer; there is a wooden diffuser and a hole (10 mm× 10 mm square and 3 mm deep) to embed the diffuser in the second layer; the third layer is the gas positioning layer (1.5 mm in diameter). The purpose of the positioning layer is to confine the injected gas so that the bubbles are generated only in this area; the bottom layer is the gas channel (1 mm in width and 0.5 mm in depth). During the chip processing, a poly(methyl methacrylate) (PMMA) mold was first engraved with a computer numerical control (CNC) engraving machine (EGX-400, Roland Inc., Japan). Then, PDMS (Sylgard 184A, 184B, Sil-More Industrial Ltd., USA) was mixed at a reagent A-to-reagent B ratio of 10:1 and degassed. The PDMS was

then poured into the engraved acrylic mold and baked in an oven at 80 °C for 30 min. Next, the wooden diffuser was embedded into the diffuser hole in the second layer, and the four PDMS layers were bonded together with O_2 plasma (PDC-001, HARRICK PLASMA, USA) to complete the chip. Figure 2(b) is a photograph of the assembled chip in which the microchannel with the red ink is the wash buffer channel, and the microchannel with the green ink is the channel for injecting air to generate bubbles. The dimensions of the entire chip were approximately 3 cm×7 cm.

2.2 Bead-based enzyme-linked immunofluorescent analysis and sample preparation

The conventional sample incubation of an enzyme-linked immunosorbent assay (ELISA) is time-consuming. Therefore, the bubble-driven micromixer was combined with a bead-based ELISA to quantitatively analyze a common protein in bladder cancer patients' urine. It is expected that this method can reduce the time of the entire analysis. Figure 3 describes the operational procedure for the bead-based enzyme-linked immunoassay. The steps are as follows: (a) first, magnetic beads coated with the primary antibody are mixed with the sample that contains the protein to be measured; (b) non-specific proteins are washed away by applying a strong magnetic field to fix the magnetic beads in place, while the unbound antigens are washed away with wash buffer; (c) the secondary antibody-biotin complex is injected for the fluorescent labeling in the next step; (d) excessive antibodies are washed away; (e) a fluorescent dye, FITC-streptavidin complex, is injected to bind the secondary antibodies and label them with fluorescence; (f) excessive fluorescent dye is washed away, and the protein concentration can be obtained by measuring the fluorescence intensity with a fluorescence microscope.

Commercial ELISA kits (Mabtech, Nacka Strand, Sweden) were used to quantitate APOA1 via an ELISA. Phosphate-buffered saline (PBS), bovine serum albumin (BSA) and the surfactant Tween-20 were purchased from Sigma-Aldrich Co. The surface of the magnetic beads (M-270 Epoxy, Dynabeads, Invitrogen) already had epoxy groups and could be coated with antibody. When coating the beads, $1.5×10^7$ beads were mixed with 4.5 μL of antibody, 95.5 μL of phosphate buffer and 50 μL of 3 M ammonium and then incubated in an oven at 37 °C for 14–16 h. Then the magnetic beads were washed with blocking buffer (PBS, 0.05 % Tween-20, 0.1 % BSA).

2.3 Operational procedure and experimental set up

The procedures of the experiment were as follows: first, the magnetic beads (30 μL) and analyte (30 μL) were injected into the reaction well with a pipette; then gas was injected quantitatively with a syringe pump (LEGATO 180, KD
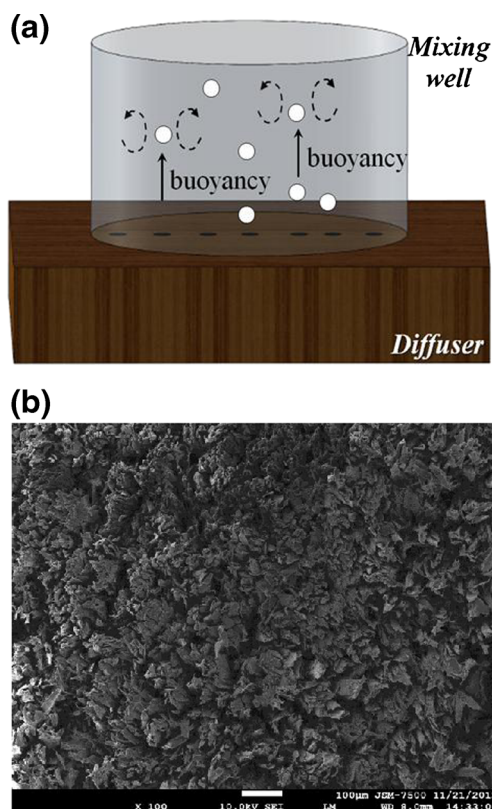
Fig. 1 a Schematic of the principle of a bubble-driven mixer. Air is steadily injected into the microfluidic chip and passed through a wooden diffuser at the bottom of the chip. The air is dispersed by the fine pores inside the diffuser to generate groups of bubbles with a diameter of less than 0.3 mm. The bubbles are raised by buoyancy and thus drive the convection in the solution. **b** SEM image of the wooden diffuser. The micrograph indicates that the internal pores are a couple hundred nanometers to tens of micrometers in diameter
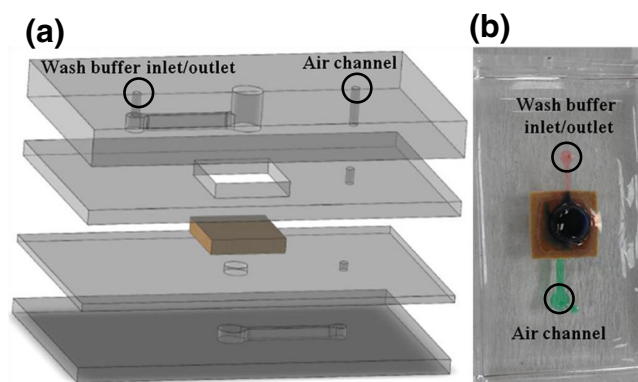

Fig. 2 a Expanded drawing of the chip composition. The chip consists of four layers of PDMS structure and a wooden diffuser. From top to the bottom, the first layer is the chip mixing well, which is connected with a microchannel. This channel is for extracting waste and injecting wash buffer; the second layer consists of a wooden diffuser and the hole for embedding the diffuser; the third layer is a gas positioning layer, to confine the position of the bubble generation; the gas channel for the bubble generation is in the bottom layer. **b** Photograph of the chip sample. The channel for the wash buffer and waste extraction is in red; the solution mixing zone is in blue; the gas channel is in green. The dimensions of the entire chip are approximately 3 cm by 7 cm

Scientific, USA) at 80 mL/h for the fine bubble generation. The antibody and antigen were bound due to the binding specificity between them. After 8 min of mixing, the sample incubation was completed, and the magnetic beads were fixed in place on the channel wall by a strong magnet (approximately 300 Gauss); next, a syringe pump matching the two-way fluid valve (connected to the inlet/outlet channel) extracted excessive unbound antigen through the microchannel that connects the mixing well (as shown in Fig. 4). The two-way valve was then turned toward the wash buffer syringe, and wash buffer was injected with another syringe pump (the extracted waste passed through the same channel as the injected wash buffer to simplify the chip design). To enhance the washing performance, the bubbles were generated for 15 s in each washing step, and each washing was repeated 3 times to ensure complete cleansing. Then, the same procedure was repeated with the secondary antibody and the fluorescent dye. At the end of the assay, the fluorescence intensity was measured with a fluorescence microscope (BX43, Olympus, Japan) combined with a photomultiplier tube (PMT) (H9305-04, Hamamatsu, Japan), and the analog signals were converted to digital signals with a data acquisition system (DAQ) (USB-6281, National Instruments, USA).

3 Experimental results

3.1 Flow rate selection for driving the micromixer and characterization of the bubble-driven mixer performance

Before using a bubble-driven micromixer, the gas-injection flow rate should be determined. The factors that must be considered when determining this flow rate are that a stable fine bubble and flow field should be generated, the time between the application of the air pressure and the generation of bubbles should not be too long and the fluid in the reaction zone should not overflow. Therefore, five different gas flow rates were utilized to observe the mixer and its behavior in bubble generation. Table 1 illustrates the relationship between the gas flow rate and the start-to-bubble-generation time. The table indicates that when the gas flow rates were 25, 50, 100, 200 and 400 mL/h, the start-to-bubble-generation times were 46.6, 23.1, 11.2, 5.8 and 3.0 s, respectively. The two parameters were approximately inversely proportional to each other. Because the gas was first injected into a PDMS chamber and then rose to pass through the diffuser before generating the fine bubbles. It can be inferred from the results that the gas pressure in the PDMS chamber had to reach a certain level before the gas could break through the fluid resistance of the diffuser to generate the fine bubbles. It was also observed in the experiment that the bubbles just emerging from the diffuser had a similar size under different gas flow rates. Larger bubbles
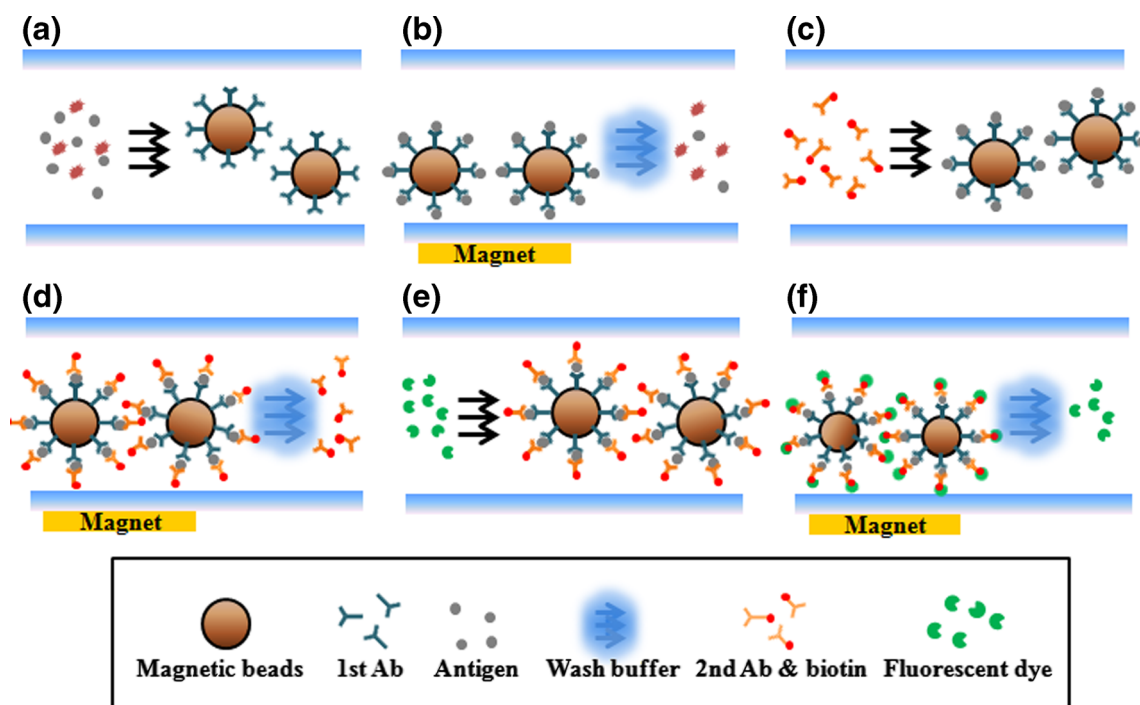
Fig. 3 The principle of the bead-based ELISA. **a** The magnetic beads coated with the primary antibody are mixed with the solution containing the biomarker to be detected. The biomarker is caught by the magnetic beads because of the binding specificity between the antibody and antigen. **b** The unbound nonspecific proteins are washed away. A strong external magnet is used to fix the magnetic beads, and the wash buffer (PBST) is injected for the wash. **c** The secondary antibody-biotin complex is injected for the subsequent fluorescent labeling. **d** Excessive secondary antibodies are washed away. **e** The analyte is labeled with fluorescence. The fluorescent dye, FITC-streptavidin complex, is injected to bind the secondary antibodies. **f** The unbound FITC is washed away

were generated only by the collision and merging of bubbles when the bubbles were generated at a high rate due to the high gas flow rate. If the bubbles were generated too quickly, merged bubbles were generated, the fluid in the mixing well

Fig. 4 Experimental set up. Two syringe pumps together with a two-way valve were used to control the wash buffer injection and waste extraction. Another syringe pump injected air at a fixed rate, which served as a stable air source for the bubble-driven mixer. After the entire magnetic bead immunofluorescence analysis was completed, the optical signal was converted to an electrical signal using a fluorescence microscope fitted with a PMT and a DAQ card

could easily overflow to the chip surface. This overflow could lead to alterations in the quantity of the analyte and to experimental error. Therefore, a moderate gas flow rate of 80 mL/h was used to drive the micromixer in the following magnetic bead immunofluorescence assay experiments. Under this flow rate, the gas-injection-to-bubble-generation time was approximately 15 s, which did not cause excessive delays in the experiment. In this experiment, it was also found that the size of the pores between the fibers in different wooden diffusers were also different, resulting in certain differences in the times required to generate bubbles. The generated bubble size may be influenced accordingly. However, it was difficult to measure the exact change of the bubble size because the percentage of change was very small. Overall, the product of the gas flow rate and the time to generate bubbles varied by approximately 20 % among mixers made of different wooden diffusers.
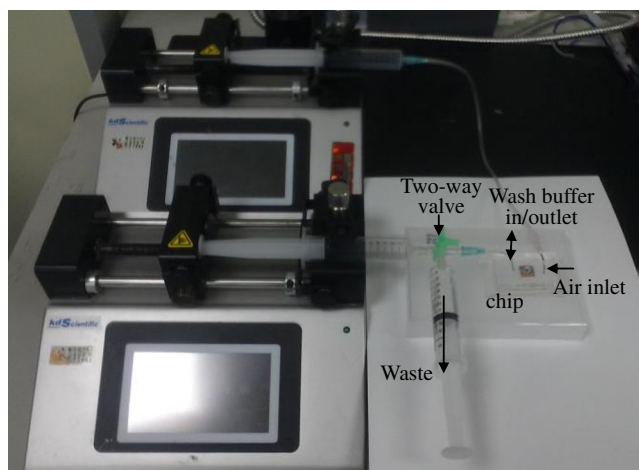
Dyes and deionized (DI) water were used to quantitatively evaluate the mixing efficiency of the bubble-driven mixer. DI water and dye were added to the reaction well, and gas was applied at 80 mL/h to drive the mixer. Figure 5(a) illustrates the dye distribution at 0, 2, 5 and 10 s of mixing. The figure shows that the gas injected into the chip was dispersed into fine bubbles of less than 0.3 mm in diameter. These bubbles caused a disturbance and convection in the fluid, which accelerated the mixing of the fluids. There were relatively

Table 1 The relationship between the gas injection flow rate and the time required to generate bubbles. The gas injection flow rate was changed from 25 to 50, 100, 200 and 400 mL/h and the corresponding times required to generate bubbles were 46.6, 23.1, 11.2, 5.8 and 3.0 s, respectively

Gas flow rate (ml/h)	400	200	100	50	25
Time required to start bubble generation (s)	3.0	5.8	11.2	23.1	46.6

large bubbles on the fluid surface. According to this observation, these bubbles were formed by the collision and merging of the small bubbles generated by the diffuser. Image analysis software, ImageJ, was used to analyze the images. A fixed area (indicated as white dot box in Fig. 5(a)) was chosen to be quantitatively analyzed, which covered the junction of the water and the dye. Then, this area was divided into 20 sections. Each section was first integrated and converted to grayscale (0–255) and then normalized to a range (0–1). After mixing, the above analysis was repeated in the same position of the image with the same fixed area, and the corresponding mixing index was calculated with Eq. (1) (Yang et al. 2009a):

$$\rho(A) = \left(1 - \frac{\int_A |C^+ - C_\infty^+| dA}{\int_A |C_0^+ - C_\infty^+| dA} \right) \times 100\% \qquad (1)$$

where $\rho(A)$ is the mixing index of the normalized concentration (C^+) distributed within the sample mixing unit (A). C_0^+ is the initial condition in the unmixed state and C_∞^+ is the completely mixed state of the normalized concentration (i.e., 0.5). Figure 5(b) is the dye concentration distribution map from the analysis of the images at 0 and 10 s. In the figure, the horizontal axis (D^+) is a fixed area at the junction of the DI water and the dye; the vertical axis (C^+) is the normalized concentration after image analysis. The data were inserted into Eq. (1) and calculated. The result indicates that the mixing index rose from 30 % to 90 % within 10 s, confirming the high mixing efficiency of this mixer. In particular, the initial 30 % mixing index was due to the diffusion of fluid molecules. In addition, it was observed that the uniformity of bubble size would not influence the mixing efficiency. However, for the stable generation of the bubbles, the applied gas flow rate was kept at 80 mL/h.

3.2 Mixing time optimization for the bead-based immunofluorescence assay

The bubble driven micromixer was integrated into a microfluidic chip to measure the concentration of a protein (APOA1) with a bead-based immunofluorescence assay. Studies have found that the concentration of this protein in urine is highly correlated with bladder cancer (Chen et al. 2010). All of the incubation steps in a conventional ELISA require more than 1 h. Therefore, the time for the entire analysis was expected to be dramatically shortened by using this

bubble-driven mixer to perform the ELISA. The optimization tests were performed with five different mixing times (1, 2, 4, 8 and 16 min) to determine the optimal incubation time when conducting the test on the chip. The abovementioned mixing times refer to the time for each incubation step in the same test. For example, a 1 min mixing time means that all of the mixing in the same ELISA test was set to 1 min. The test was performed with three different concentrations of APOA1 (200, 100 and 50 ng/mL) to evaluate its reproducibility.
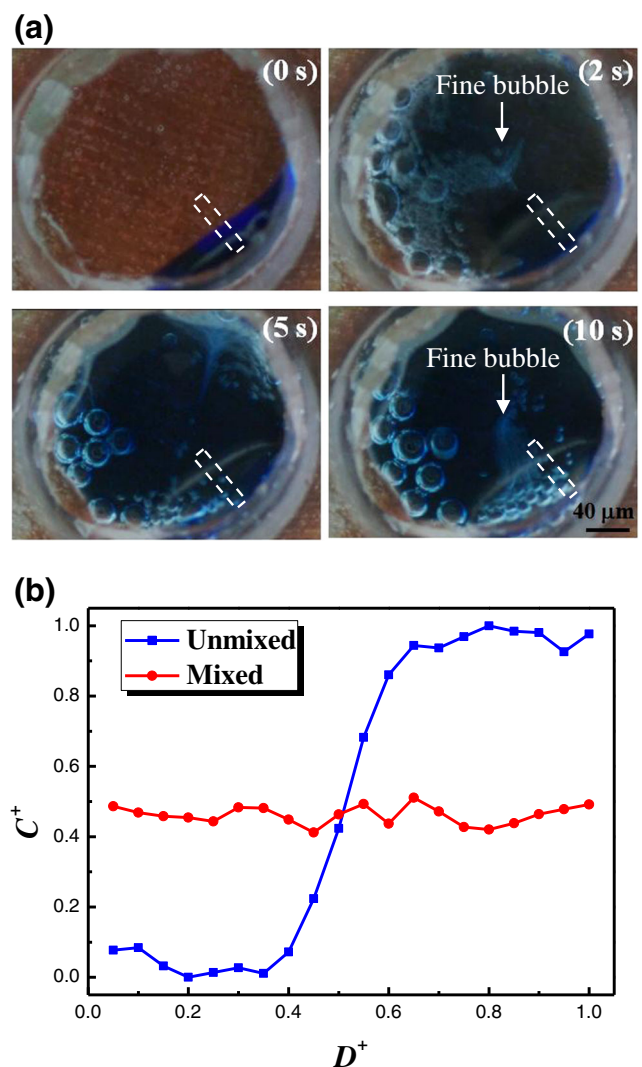

Fig. 5 Bubble-driven mixer efficiency characterization. **a** Series of photographs of the mixer actuated for a period of 10 s. The ink and DI water were mixed together gradually; **b** Concentration distribution map of dye mixing. D+ denotes a certain area in the blue ink and clear water junction; C+ denotes the normalized concentration after image analysis

Figure 6(a) illustrates the relationship between the mixing time and the fluorescence intensity. The figure indicates that the fluorescent signal increased with increasing mixing time. If the fluorescent signal measured after 16 min mixing was set to 100 % for each concentration, then the relative signal strengths after 8 min of mixing were 97.8 %, 98.4 % and 94.6 % for protein concentrations of 200 ng/mL, 100 ng/mL and 50 ng/mL, respectively. These values nearly approached those obtained after 16 min of mixing. In addition, to confirm the result of optimization of mixing time, we carried out another trial that used bead-based ELISA with enzyme labeling. All of the experimental procedures are the same as enzyme-linked immunofluorescent analysis described above, except for the development of the enzyme. The development (reaction between enzyme and substrate) time was set to be 30 min for all measurement and the reagents were suspended to measure the optical density at 405 nm. The trends are the same with the enzyme-linked immunofluorescent analysis (data not shown here). In contrast, without the bubble actuation, the immunoassay signal from three concentrations samples did not become saturated even if the incubation time was as long as 120 min. The optical intensities of the three concentration samples were slightly increased and showed no significant difference, which indicated that the incubation was not completed (Fig. 6(b)). Therefore, we set the optimal mixing time to 8 min. Compared with a conventional ELISA, the time for the incubation step was reduced from 60 min to 8 min, resulting in a time reduction from 3–4 h to 30–40 min for the entire assay. If the mixing time of traditional ELISA was set to be 8 min, the detection signal would be very low and the low concentration of protein (lower than 12.5 ng/mL) could not be measured with short time incubation (data not shown).

3.3 Detection range and limits for a bladder cancer biomarker

The APOA1 concentration can be up to approximately 7,000 to 8,000 ng/mL in a bladder cancer patient's urine sample (Chen et al. 2010). Therefore, the APOA1 concentration in the standard solution prepared in our study ranged from 0 ng/mL to 9,000 ng/mL, with an increment interval of 1,000 ng/mL, to evaluate the maximum concentration that the system could analyze. Figure 7(a) shows the relationship between the APOA1 concentration and the detected concentration derived from the fluorescence signal. The signal shown for each concentration is the mean and the error of three replicate experiments. The figure indicates that a linear coefficient (R^2) of up to 0.973 was obtained from the curve fitting (least-squares linear regression) of the detected signals for concentrations of 0 to 9,000 ng/mL. The amount of magnetic beads was 7.5 μl (1×10^8 beads/mL). This measurement range was 200 times larger than the range in the calibration curve for the plate-based ELISA provided in the ELISA kit. This large measurement range is due to the three-dimensional structure
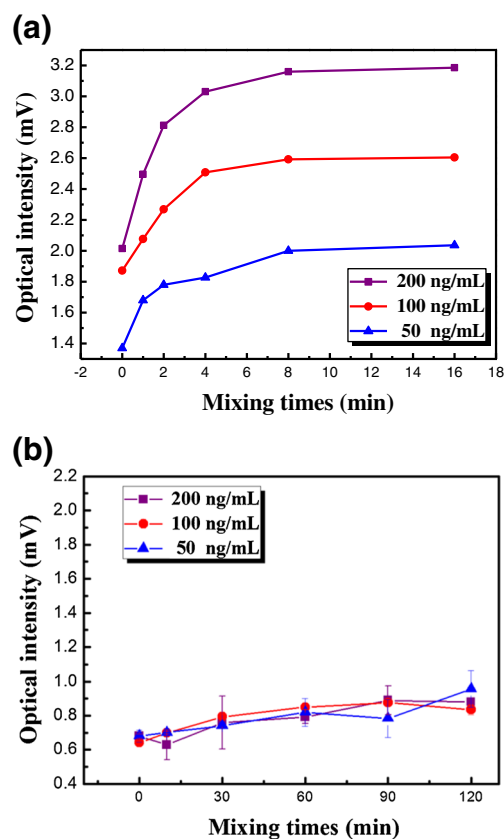

Fig. 6 **a** Incubation time optimization for the on-chip bead-based immunofluorescence assay. Three different concentrations of the APOA1 antigen (50, 100 and 200 ng/mL) were used in the experiment, and the bubble-driven mixer was used for the incubation. The mixing times (the time required by each incubation step in the same ELISA test) were 0, 1, 2, 4, 8 and 16 min. The signal strength approached the maximum after 8 min of mixing for all three analyte concentrations. **b** The characteristic signal on rate without the bubble actuation. Even if the mixing time was increased to 120 min, the signals did not reach its plateau

of the magnetic beads; much more antibody can be coated onto the beads' surface than onto the bottom surface of a 96-well plate, resulting in a much larger detection range of analyte concentrations. In a practical application, our system can detect analytes in samples without dilution, even though the APOA1 concentration in a patient's urine can reach 7,000 to 8,000 ng/mL. In contrast, the plate-based ELISA requires two to three ten-fold serial dilutions to obtain an analyte concentration that is within the range of the standard curve before any test can be performed. This serial dilution consumes reagent and thus may cause errors during operation. Therefore, the proposed method can reduce the amount of reagent used and the testing time for biomarker measurement.

If an antigen can be detected at low concentrations, then biomarker detection at the early stage of cancer is possible, and early diagnosis and early treatment are achievable. Therefore, tests on the limit of detection (LOD) were performed in our study. The APOA1 concentration was diluted from 80 ng/mL to 1.25 ng/mL with two-fold serial

dilutions. Equation (2) was used to calculate and verify the LOD obtained from the experiment (Hayashi et al. 2004; Rajakovic et al. 2012),

$$LOD = 3.3 \times (s/f') \tag{2}$$

where s is the standard deviation when the concentration of the test sample is zero, i.e., the background noise and f' is the slope of the calibration curve. Figure 7(b) contains the result of the LOD measurement. The data for each concentration was the average of three replicate experiments. The results indicate that a LOD of 9.16 ng/mL was derived from both experimental results and theoretical calculations. This value is lower than the cut-off value (11.16 ng/mL, $n=126$, 94.6 % sensitivity and 92.0 % specificity, Chen et al. 2010) used in bladder cancer diagnosis based on the APOA1 concentration in urine. Note that the value 11.16 ng/mL is a temporal landmark for the experiment, which was provided by our cooperation research group of Molecular Medicine Research Center in Chang Gung University. The exact cut-off value for bladder cancer diagnosis needs to be further verified by other investigations.

However, some issues regarding diffuser's material need to be solved, which might improve the detection accuracy and detection limit. Materials with fine texture would absorb the analyte due to capillary force. We have tried two kinds of material for the gas diffuser: one is wood and the other is ceramic. Both of them have the problem of retaining analyte. We observed that the ceramic one has a more severe problem than wood in absorbing analyte. Therefore, we used wood as the diffuser material. In practice, prior to introducing the analyte for the experiment, 30 µl blocking buffer was injected into the reaction chamber. This step can avoid the absorption of analyte in the wooden texture but may cause some measurement error. Perhaps the use of hydrophobic layer coating on the wood or other material can further solve this problem. For example, polyurethane membrane (refer to AEROSTRIP®) and EPDM membranes (refer to Viton®) are popular materials for generating fine bubbles in industry aeration technology. These kinds of polymer-based material may not retain the analyte as much as wood or ceramic.

4 Conclusions

A bubble-driven mixer with a simple design and simple fabrication was deployed in our study. The mixer adopted a wooden diffuser to refine the air and used buoyancy to raise the bubbles to mix the fluids. The mixing index indicated that this micromixer could effectively mix clean water and dye within 10 s (the mixing index rose from 30 % to 90 %). The mixer was integrated into a microfluidic chip and used for a bead-based ELISA. The system could effectively detect
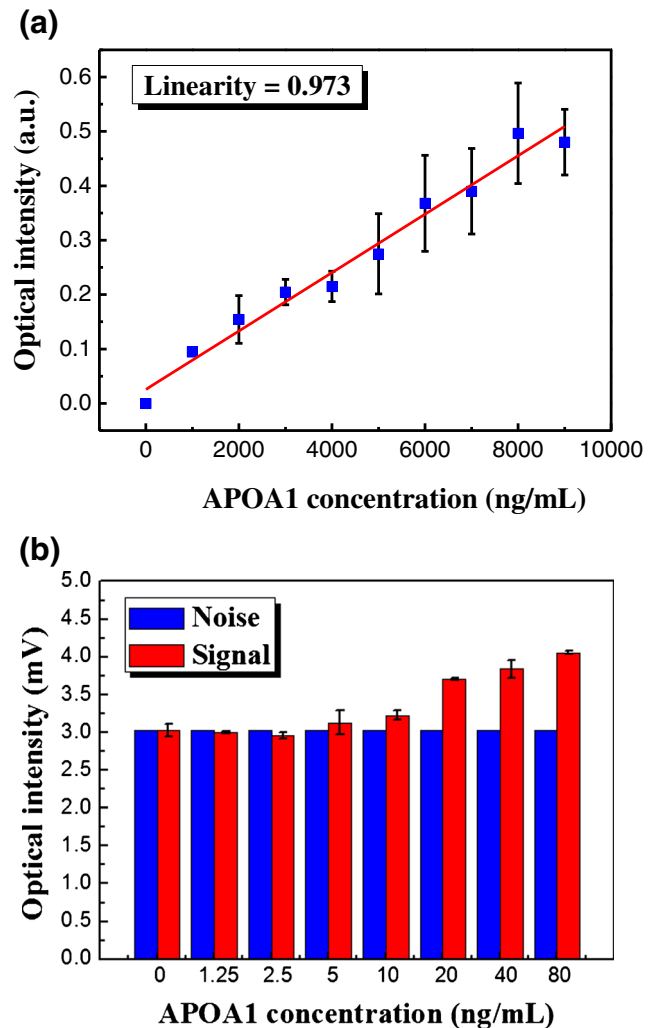
(a)

(b)

Fig. 7 a The detection range of the bubble-driven mixer-integrated microfluidic chip for a bladder cancer biomarker. **b** The detection limit of the proposed microfluidic chip for a bladder cancer biomarker

APOA1, the biomarker in bladder cancer patients' urine, by exploiting the three-dimensional surface area of the magnetic beads for effective antibody coating. The detection range was 0 to 9,000 ng/mL, which eliminates the need to dilute a patient's urine sample. In addition, the system LOD was measured to be 9.16 ng/mL, which was also lower than the bladder cancer diagnosis cut-off value of 11.16 ng/mL reported in the literature. The chip detection only required 30 to 40 min compared with the 3 to 4 h required for a conventional ELISA. Hopefully, this system will be used as of point-of-care method for bladder cancer detection in the future.

Conflict of interest The authors declare that they have no conflict of interest.

References

D. Ahmed, X. Mao, B.K. Juluri, T.J. Huang, Microfluid. Nanofluid. **7**, 727 (2009)

P.A. Auroux, D. Iossifidis, D.R. Reyes, A. Manz, Anal. Chem. **74**, 2637 (2002)

Y.T. Chen, C.L. Chen, H.W. Chen, T. Chung, C.C. Wu, C.D. Chen, C.W. Hsu, M.C. Chen, K.H. Tsui, P.L. Chang, Y.S. Chang, J.S. Yu, J. Proteome Res. **9**, 5803 (2010)

Y.T. Chen, H.W. Chen, D. Domanski, D.S. Smith, K.H. Liang, C.C. Wu, C.L. Chen, T. Chung, M.C. Chen, Y.S. Chang, C.E. Parker, C.H. Borchers, J.S. Yu, J. Proteomics **75**, 3529 (2012)

P. Garstecki, M.J. Fuerstman, M.A. Fischbach, S.K. Sia, G.M. Whitesides, Lab Chip **6**, 207 (2006)

Y. Hayashi, R. Matsuda, T. Maitani, Anal. Chem. **76**, 1295 (2004)

M. Herrmann, E. Roy, T. Veres, M. Tabrizian, Lab Chip **7**, 1546 (2007)

P.I. Karakiewicz, S. Benayoun, C. Zippe, G. Lüdecke, H. Boman, M. Sanchez-Carbayo, R. Casella, C. Mian, M.G. Friedrich, S. Eissa, H. Akaza, H. Huland, H. Hedelin, R. Rupesh, N. Miyanaga, A.I. Sagalowsky, M.J. Marberger, S.F. Shariat, BJU Int. **97**, 997 (2006)

D.S. Kim, S.H. Lee, T.H. Kwon, C.H. Ahn, Lab Chip **5**, 739 (2005)

D.S. Kim, S.W. Lee, T.H. Kwon, S.S. Lee, J. Micromech. Microeng. **14**, 798 (2004)

H. Li, C. Li, H. Wu, T. Zhang, J. Wang, S. Wang, J. Chang, Proteome Sci. **9**, 1 (2011)

Y.H. Lin, Y.J. Chen, C.S. Lai, Y.T. Chen, C.L. Chen, J.S. Yu, Y.S. Chang, Biomicrofluidics **7**, 024103 (2013)

M. Lindén, S.B. Lind, C. Mayrhofer, U. Segersten, K. Wester, Y. Lyutvinskiy, R. Zubarev, P.-U. Malmström, U. Pettersson, Proteomics **12**, 135 (2012)

R.H. Liu, J. Yang, M.Z. Pindera, M. Athavale, P. Grodzinski, Lab Chip **2**, 151 (2002)

R.H. Liu, R. Lenigk, R.L. Druyor-Sanchez, J. Yang, P. Grodzinski, Anal. Chem. **75**, 1911 (2003)

Y. Lotana, C.G. Roehrborna, Urology **61**, 109 (2003)

L.H. Lu, K.S. Ryu, C. Liu, J. Microelectromech. Syst. **11**, 462 (2002)

X. Mao, B.K. Juluri, M.I. Lapsley, Z.S. Stratton, T.J. Huang, Microfluid. Nanofluid. **8**, 139 (2010)

K.G. McKenzie, L.K. Lafleur, B.R. Lutz, P. Yager, Lab Chip **9**, 3543 (2009)

D. Mitropoulos, A. Kiroudi-Voulgari, P. Nikolopoulos, T. Manousakas, A. Zervas, J. Endourol. **19**, 861 (2005)

L.V. Rajakovic, D.D. Markovic, V.N. Rajakovic-Ognjanovic, D.Z. Antanasijevic, Talanta **102**, 79 (2012)

H. Suzuki, C.M. Ho, N. Kasagi, J. Microelectromech. Syst. **13**, 779 (2004)

T. Tanahashi, Y. Matsumura, H. Ohmori, T. Tanaka, Acta Med. Okayama **32**, 139 (1978)

J.H. Tsai, L. Lin, J. Microelectromech. Syst. **11**, 665 (2002)

R.A. Vijayendran, K.M. Motsegood, D.J. Beebe, D.E. Leckband, Langmuir **19**, 1824 (2003)

H. Xiao, D. Liang, G. Liu, M. Guo, W. Xing, J. Cheng, Lab Chip **6**, 1067 (2006)

S.Y. Yang, J.L. Lin, G.B. Lee, J. Micromech. Microeng. **19**, 035020 (2009a)

Y.N. Yang, H.I. Lin, J.H. Wang, S.C. Shiesh, G.B. Lee, Biosens. Bioelectron. **24**, 3091 (2009b)